Molecular Crystals and Liquid Crystals Science and Technology. Section A. Molecular Crystals and Liquid Crystals

Publication details, including instructions for authors and subscription information:
http://www.tandfonline.com/loi/gmcl19

Pattern Formation at the Nematic Smectic-B Interface

Tibor Tóth-Katona [a], Tamás Börzsönyi [a] & ágnes Buka [a]

[a] Research Institute for Solid State Physics and Optics of the Hungarian Academy of Sciences, H-1525, Budapest, P.O.B. 49, Hungary

Version of record first published: 24 Sep 2006

To cite this article: Tibor Tóth-Katona, Tamás Börzsönyi & ágnes Buka (2000): Pattern Formation at the Nematic Smectic-B Interface, Molecular Crystals and Liquid Crystals Science and Technology. Section A. Molecular Crystals and Liquid Crystals, 339:1, 175-208

To link to this article: http://dx.doi.org/10.1080/10587250008031042

Mol. Cryst. Liq. Cryst., Vol. 339, pp. 175-208
Reprints available directly from the publisher
Photocopying permitted by license only

Pattern Formation at the Nematic Smectic-B Interface

TIBOR TÓTH-KATONA*, TAMÁS BÖRZSÖNYI and ÁGNES BUKA

Research Institute for Solid State Physics and Optics of the Hungarian Academy of Sciences H-1525 Budapest, P.O.B.49, Hungary

(Received January 04, 1999; In final form July 26, 1999)

Free growth properties of the smectic B liquid crystalline phase into the supercooled nematic have been investigated in quasi-twodimensional geometry. Different orientation combinations of the two phases have been achieved experimentally and the interfacial patterns have been studied and analysed as a function of undercooling. The angular dependence of the surface tension has been deduced from the shape of the interface in thermal equilibrium. The experimentally determined surface tension anisotropy has been incorporated into computer simulations based on the phase-field model. The simulations have reproduced qualitatively the rich variety of morphologies observed in the experiments for a given set of undercoolings in three geometries. Anisotropic heat diffusion on the nematic side, relevant to our experimental system has also been introduced. Both in the experiments and in the simulations we find that the growth is faster in the lower heat diffusion direction.

Keywords: pattern formation; phase transition; liquid crystals

INTRODUCTION

Interfacial patterns in the process of solidification (see e.g. [1, 2, 3, 4]) typically posses characteristical length scales of $10 - 100\mu m$ that roughly define the microstructure of the emerging solid phase and implicitly influences its mechanical-, chemical-, thermal-, and other properties. Therefore, the understanding of this pattern forming process besides of academical aspects has practical importance too in designing materials of application tailored properties. On this scale the ordering and motion on atomic level can be neglected, the solid and liquid phases can be treated as continuous medium. In this approach the solidification problem can be described as a first order phase transition i.e., as a process in

* Correspondence author. E-mail:katona@power.szfki.kfki.hu Phone: (36–1) 395–9220 Fax: (36–1) 395–9278

which latent heat (L) is released and conducted away from the interface. In the further discussion we will restrict ourselves to two dimensions. In one-component crystal – melt systems (if one neglects the convection) the released heat will be transported by diffusion:

$$D_{1,2}\nabla^2 T_{1,2} = \frac{\partial T_{1,2}}{\partial t}; \tag{1}$$

where: numbers 1 and 2 denote the crystal and the liquid phase, respectively; D_1, D_2 – heat diffusion coefficients of the two phases; T_1, T_2 – temperatures (variable in space and time) on the two sides of the interface.

The melt is undercooled by $\Delta T = T_m - T_\infty$, so the temperature in the liquid phase, far from the interface is given by: $T_\infty = T_m - \Delta T$, while in the crystal phase the temperature is nearly T_m, where T_m is the phase transition temperature.

Since the location of the interface is free, an extra boundary condition has to be given, which describes the local thermodynamic equilibrium of the front and takes into account the Gibbs-Thomson relation and the kinetic effects (taken in the description as a linear effect):

$$T_i(s,t) = T_m[1 - \tilde{d}_0(\theta)\kappa(x,t)] - \frac{1}{\tilde{\mu}(\theta)}v_n \tag{2}$$

where: $T_i(s, t)$ – the temperature of the interface, $s = s(x, y)$ – the equation of the interface, $\kappa(x, t)$ – the curvature of the interface, and

$$\tilde{d}_0(\theta) = \tilde{\sigma}(\theta)/L = [\sigma(\theta) + \sigma''(\theta)]/L \tag{3}$$

is the capillary length ($\sigma(\theta)$ – surface tension, θ – angle enclosed by the normal of the interface and an arbitrary direction).

On the basis of the Gibbs-Thomson correction of the phase transition temperature, a circular crystal with radius R is in thermal equilibrium with its melt at the temperature $T = T_m(1 - \tilde{d}_0/R)$ (see e.g. [5]). In general, when the surface tension is anisotropic, the so called surface stiffness $\tilde{\sigma}(\theta)$ appears in the Gibbs-Thomson relation (see e.g. [6]).

The last term in the equation (2) describes the kinetics of the interface, where: $\frac{1}{\tilde{\mu}(\theta)} > 0$ – is the kinetic coefficient, v_n – the normal velocity of the interface. In general, the front kinetics is also direction dependent (as the $\sigma(\theta)$), because particles (atoms, molecules) can enter the crystal from the melt with different efficiency from different directions.

From the energy conservation principle: the latent heat released at the interface must be equal to the sum of the heat flows from and to the interface i.e.,:

$$\frac{v_n L}{c_p} = (D_2\partial_n T_2 - D_1\partial_n T_1) \tag{4}$$

where: $\partial_n T_1$ and $\partial_n T_2$ are the normal temperature gradients on the two sides of the interface, and c_p is the specific heat.

For a given undercooling ΔT, the material parameters D, $\sigma(\theta)$, $\frac{1}{\tilde{\mu}(\theta)}$, L and c_p determine whether the interface remains stable or becomes unstable during its motion. The surface tension and its anisotropy plays an important role in the selection of the growth morphology of the interface (see e.g. [4]). Without the stabilizing effect of the surface tension (in the limit of $\sigma(\theta) \to 0$) the temperature field destabilizes the interface and the growth morphology becomes fractal. In the presence of an isotropic σ the interplay between the effects of the temperature field and σ leads to the so called dense-branching morphology through tip-splitting. For the stable dendritic growth surface tension anisotropy (or at least anisotropy in the interface kinetics) is necessary.

A great number of experiments were done on traditional solid-liquid systems [7, 8, 9, 10, 11]. Most of these crystal – melt systems have relatively small anisotropy:

$$\varepsilon = \frac{\sigma_{max} - \sigma_{min}}{\sigma_{max} + \sigma_{min}} \tag{5}$$

(only few %) in the surface tension. In contrast, liquid crystalline (LC) systems, as it has been shown previously for the smectic-A (Sm-A) – smectic-B (Sm-B) [12] and for the nematic (N) – Sm-B [13] phase transitions, can have much larger ε with expressed facets in the equilibrium shape of the interface. Moreover, in these systems ε can differ by an order of magnitude in different planes of observations with respect to the symmetry axes of the LC phases.

The N – crystalline Sm-B phase transition (smectification), we studied, is the liquid crystalline analogy of solidification of a pure substance, that is of first order with a latent heat typically $L = 4 - 8 kJ/mol$ [14].

Liquid crystals differ from the isotropic melt – crystal systems in the heat diffusion too. The heat diffusion coefficient D is anisotropic both for the nematic (which plays the role of the melt in our observations) and for the smectic phases:

$$D_a = \frac{D_{\parallel} - D_{\perp}}{D_{\perp}} \tag{6}$$

where: $D_{\parallel}$ and $D_{\perp}$ – diffusion coefficients parallel and perpendicular to the director $\mathbf{n}$ (that describes the orientation of the phase), respectively.

Analysing experimental data of D for a number of LC materials, we can assume some general features of the heat transport:

- $D_a > 0$ for nematics and it remains positive also in smectic phases [15], contrary to the mass- and electric transport processes, where the anisotropy changes sign at the nematic – smectic transition.

- The magnitude of the average heat diffusion coefficient D and that of D_a in the Sm-B phase do not differ significantly from those in the N phase – see for example [16, 17, 18];
- The contribution of the rigid central core of the molecule to the thermal diffusivity is more important than that of the aliphatic end chain [18]. The increase of the alkyl-chain length by one or two carbon atoms does not affect the magnitude of D significantly [16, 17].
- D_a depends strongly on the molecular shape. At fixed molecular width, it increases with molecular length. D_a depends primarily on the length of the rigid core [15], but the increase of the alkyl-chain length by one or two carbon atoms increases D_a also [16, 17, 18].

Besides the surface tension anisotropy (that is extremely large in some geometries and involves expressed facets in the equilibrium shape of the interface), the anisotropy in the heat diffusion of the N phase was the main subject of our experimental and numerical studies. The ε tunable in a wide range (by ensuring different orientations of the two phases, or by choosing different LC materials) gave the possibility of exploring its role in the interface evolution from the first destabilization to fully developed dendrites. Moreover, the heat diffusion anisotropy was incorporated in the governing equations and its counter-intuitive effect on the pattern formation was studied both experimentally and numerically.

In this work after a brief introduction of the phase-field model and of the experimental setup, we review the properties of the N – Sm-B interface in thermal equilibrium for different director alignments and for different substances. We also give the angular dependence of the surface tension extracted from the equilibrium shape of the interface. The growth properties are summarized in three sections as a function of the undercooling for different director alignments and for different substances (including binary mixtures). A separate section deals with a peculiar effect specific to some LC materials i.e., with thermally induced aging. Results concerning the effect of the heat diffusion anisotropy on the pattern formation are presented also in a separate section, as well as the inverse process i.e., melting of the Sm-B phase.

THE PHASE-FIELD MODEL

In the "*diffusion model*" of solidification described in the previous section, the most important variable is the temperature field. The model takes into account the latent heat released during solidification and its diffusion, but neglects some microscopic properties of the process: the interface is assumed to be sharp ($\delta = 0$,

δ – the thickness of the interface), furthermore the model assumes that the interface is in local thermodynamic equilibrium.

Contrary to the diffusion model, the "*order-parameter model*" of solidification (see e.g. [19, 20]) gives an equation for the order parameter that distinguishes the two phases. In this model the temperature field is assumed to be the same in the whole system and constant in time (the released L and its diffusion is neglected). In the same time, the model takes into account some microscopic properties of the solidification as the finite interface thickness δ, the kinetic time-scale (which controls the dynamics of the fluctuations) and variations from the thermodynamical equilibrium (that cause the motion of the interface).

Keeping the most important features of these two models, one can construct a model where a new parameter ϕ is coupled to the temperature field. This *phase-field* model has been introduced by Halperin, Hohenberg and Ma [21, 22], and it has been modified by Langer [23] for the solidification problem taking into account the Gibbs-Thomson relation. In the model the order parameter ϕ describes the difference between the two phases. In the vicinity of the interface ϕ changes continuously in space forming a smooth boundary between the solid and liquid phases. In contrast to the sharp interface model, here the interface has a finite thickness δ which is a new parameter of the model and which in the limit $\delta \to 0$ assures the convergency to the sharp interface model [24, 25]. The dynamics of ϕ is derived from the variation of a Ginzburg-Landau type free energy (or entropy) functional. Through the relaxation character of the dynamics of ϕ the kinetic effects can be incorporated into the model and their magnitude can be controlled with the relaxation time. The anisotropies of $\sigma(\theta)$ and $\frac{1}{\mu(\theta)}$ can be also incorporated easely.

After its introduction the analitical properties of the model (proposed by Langer) have been studied intensively [24, 26, 27, 28, 29]. The numerical method has been introduced by Fix [30], and at the beginning the simulations have been carried out in one dimension only [31, 32, 33]. At the beginning of this decade the model introduced by Kobayashi [34] gave the possibility for numerical simulations of solidification processes in two- [35] and in three-dimensions [36]. A slightly different model has been proposed by Wheeler et al. and used for the simulation of the dendritic growth of nickel [37]. Recently, Karma et al. introduced [38, 39] a modification in the phase-field model which gives the possibility to decrease the CPU-time, and enables the quantitative analysis of the interface for smaller undercoolings.

In our simulations we have used a set of equations derived in [40], where the dynamics satisfies a spatially local positive entropy production, and involves constant values of ϕ in the bulk phases (which do not depend on the undercool-

ing) resulting a correct latent heat production. In addition we have included into the model the anisotropic heat diffusion which is relevant for our LC systems. The pair of coupled equations for the phase $\phi(\mathbf{r}, t)$ and dimensionless temperature field

$$u(\mathbf{r},t) = \frac{T - T_m}{\Delta T} \tag{7}$$

is as follows:

$$\epsilon^2 \tau(\theta) \frac{\partial \phi}{\partial t} = \phi(1-\phi)\left[\phi - \frac{1}{2} + 30\epsilon\beta\Delta u \phi(1-\phi)\right] - \epsilon^2 \frac{\partial}{\partial x}\left(\eta(\theta)\eta'(\theta)\frac{\partial \phi}{\partial y}\right) + \\ + \epsilon^2 \frac{\partial}{\partial y}\left(\eta(\theta)\eta'(\theta)\frac{\partial \phi}{\partial x}\right) + \epsilon^2 \nabla(\eta^2(\theta)\nabla\phi) \tag{8}$$

$$\frac{\partial u}{\partial t} + \frac{1}{\Delta}(30\phi^2 - 60\phi^3 + 30\phi^4)\frac{\partial \phi}{\partial t} = \nabla_i K_{ij} \nabla_j u \tag{9}$$

The values $\phi = 1$ and $\phi = 0$ correspond to the liquid and solid phases, respectively. Lengths are scaled in some arbitrary length ω, while times are scaled by $\omega^2/D_\perp$. The local orientation of the front is given by:

$$tg\theta = \frac{\partial_y \phi}{\partial_x \phi} \tag{10}$$

The dimensionless parameters of the model are:

$$\Delta = \frac{c_p \Delta T}{L} \tag{11}$$

$$\beta = \frac{\sqrt{2}\omega L^2}{12 c_p \sigma(0) T_m} = \frac{\sqrt{2}\omega}{12 d_0} \tag{12}$$

$$\tau(\theta) = \frac{L D_\perp}{\sigma(0) T_m} \frac{\eta(\theta)}{\mu(\theta)} = \frac{c_p D_\perp}{L d_0} \frac{\eta(\theta)}{\mu(\theta)} \tag{13}$$

$$\epsilon = \frac{\delta}{\omega} \tag{14}$$

and

$$K_{ij} = \frac{D_{ij}}{D_\perp}. \tag{15}$$

where:

$$\eta(\theta) = \frac{\sigma(\theta)}{\sigma(0)}, \tag{16}$$

and

$$d_0 = \frac{\tilde{d}_0 T_m c_p}{L} \tag{17}$$

and

$$\frac{1}{\mu(\theta)} = \frac{1}{\tilde{\mu}(\theta)} \frac{c_p}{L}. \tag{18}$$

In this paper we give a comparison between the experiments and the phase field model simulations for the H(inH) case. For the P(inP) geometry this comparison can be found in [41, 42]. The phase-field model equations (7) and (8) have been solved numerically on a rectangular lattice. Both equations have been discretized spatially using first order finite differences on a uniform grid mesh spacing Δx. An explicit time-differencing scheme has been employed for the equation (7) and the time step Δt has been adjusted in each case in order to avoid numerical instability. The equation (8) has been solved by the alternating-direction implicit method (ADI), which is unconditionally stable [37]. We have simulated the experimental system by locating the initial Sm-B seed ($\phi = 0$, $u = 0$) in the center of the mesh. In the rest of the system $\phi = 1$, $u = -1$ have been set initially. Boundary conditions of $\phi = 1$ and $u = -1$ have been imposed on the four sides of the system. In absence of experimental data about $\frac{1}{\mu(\theta)}$, for H(in H) configuration we have taken in our simulations a sixfold anisotropy in the kinetic coefficient:

$$\frac{1}{\mu(\theta)} = \frac{1}{\mu_0}(1 + \varepsilon_{\mu 6} cos(6\theta)) \tag{19}$$

with $\varepsilon_{\mu 6} = -0.003$. This anisotropy represents an estimation given in [43].

EXPERIMENTAL SYSTEM

Different liquid crystalline substances were used for observations. Each of them has a first-order phase transition N to Sm-B at T_{NS}:

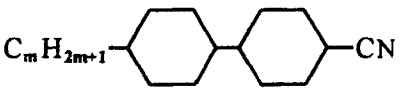

m=3: *4-n-propyl-4'-cyano-trans 1,1-bicyclohexane*, (CCH3), T_{NS}=56.3°*C*;
m=4: *4-n-butyl-4'-cyano-trans 1,1-bicyclohexane*, (CCH4), T_{NS}=53.1°*C*;
m=5: *4-n-pentyl-4'-cyano-trans 1,1-bicyclohexane*, (CCH5), T_{NS}=51.2°*C*;

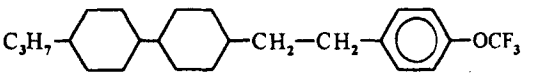

4-n-propyl-4'-trifluoromethoxyphenyl-ethylene-trans 1,1-bicyclohexane, (3OCF3), T_{NS}=77.0°C;

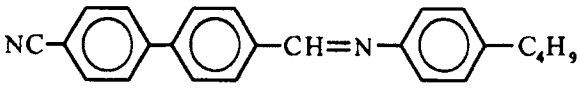

4-n-butyl-N-[4-(p-cyanophenyl)-benzilidene]-aniline, (BCBA), T_{NS}=87.4°C.

Samples of both surface alignments of the nematic phase – planar (P, $\mathbf{n} \parallel$ to the bounding glass plates) and homeotropic (H, $\mathbf{n} \perp$ to the bounding glass plates) - were prepared in cells of dimensions $\approx 20 \times 20 mm^2$ and of thickness d=10μm. For planar orientation of the nematic phase we used commercial liquid crystal cells manufactured by E.H.C. Co., Ltd. (Japan). For making cells with homeotropic orientation the glass plates with SnO_2 coating have been used. A thin layer of octadecyl-triethoxy-silane, transferred onto the inner surfaces by polymerization, assured the homeotropic alignment.

The sample temperature was controlled in a hot stage with accuracy of 0.002°C. The hot stage was mounted on a polarizing microscope equipped with CCD video camera. The recorded images were fed into a PC for digital analysis, with spatial resolution of 512x512 and 256 gray scaling for each pixel. With 6.3× objective the scale factors of 1.35±0.01μm/pixel in x direction and 0.95±0.01μm/pixel in y direction were determined, so the calculated area of the pixel is 1.28±0.02μm^2.

In the experiments both P and H orientations of the Sm-B phase could be assured, thus different director configurations of the two phases could be investigated. For easier characterisation of the system, we introduce symbols. Thus, for example in case of planarly oriented smectic germ in homeotropic nematic surrounding, we use designation P(in H), etc.

NEMATIC – SMECTIC-B INTERFACE IN THERMAL EQUILIBRIUM

Slowly heating up the Sm-B and approaching T_{NS} one can achieve a state where only a few Sm-B islands surrounded by the N phase are left and they are separated (usually far) from each other so that no interaction between them is present. Choosing one of these smectic germs for further observation and controlling the temperature (with corrections on the mK scale) in order to keep the size of the germ constant one can approach the thermal equilibrium state of this system. After a few hours of equilibration the shape of the N – Sm-B interface is stabi-

lized. Similar equilibration time (~ $1h$) has been found in the solvent of organic substance HET [44].

From the shape of the interface in thermal equilibrium we have derived the angle dependence of the normalized surface tension $\eta(\theta)$ by the Wulff-construction [45]. This is a geometrical construction based on the fact that the equilibrium shape minimizes the surface free energy.

Thermal Equilibrium with different Orientations of the Two Phases

The shape of the N – Sm-B interface has been determined in thermal equilibrium with different orientation combinations of the two phases: P(in P), P(in H) and H(in H) [46]. The H(in P) configuration has been studied for CCH5 only and the results were presented in [43].

A faceted, rectangle like, elongated shape (Fig. 1(a)and (b)) has been found for the planar Sm-B. The longer, faceted edges are parallel to the smectic layers (perpendicular to the director) indicating that the Sm-B phase consits of stiff planes (contrary to the Sm-A phase). We point out here that when a facet is present at the melt – crystal interface, it is known (see e.g. [6]) that the advance of the facet can be stucked and might happen that the experimentally determined steady shape of the interface does not reflect the real equilibrium morphology. In such cases a special care should be taken in the process of equilibration, allowing the interface to "breathe".

FIGURE 1 The shape of the N – Sm-B interface in thermal equilibrium for CCH3. (**a**) P(in P), (**b**) P(in H), (**c**) H(in H). The arrows show the director orientations in the both phases

For the shape anisotropy $(R_{max} - R_{min})/(R_{max} + R_{min})$ (R - distance of the germ perimeter from its nucleation point), which coincides with the surface tension anisotropy ε [47], in P(in P) geometry for CCH3 a value of $\varepsilon = 0.68$ has been measured. In the P(in H) configuration of CCH3 a somewhat smaller value of ε ($\varepsilon = 0.49$) has been found, due to an additional contribution to the surface energy coming from the elastic deformation of the nematic near the interface which is of splay-bend type along the long edges and mainly twist along the short ones [46].

On the basis of the experiments, the reproducibility of the ratio R_{max}/R_{min} has been estimated to be below 20% [48]. These values of ε are extremly large compared to that measured in the isotropic melt – crystal systems of other organic substances (e.g. $\varepsilon = 0.005$ for succinonitrile [9, 49], $\varepsilon = 0.006 - 0.05$ for pivalic acid [9, 49, 50, 51], $\varepsilon = 0.03$ for camphene [52] or $\varepsilon = 0.003$ for HET [53]). A similarly large value of ε has been found for the Sm-A – Sm-B interface in buthyloxybenzilidene octylanyline [12], where $\varepsilon \approx 0.5$ has been measured.

The Wulff-construction gave us the possibility to determine the function $\eta(\theta)$ (where θ describes the interface orientation) by a simple polinomial fit. In case of planar Sm-B for $\theta = 0$ we have chosen the orientation parallel with the smectic layers (perpendicular to the smectic director $\mathbf{n}(S)$). In CCH3 the following functions have been determined [54, 41]:

for P(in P): $\eta(\theta) = 1.000 - 0.352\theta^2 + 0.008\theta^4$

for P(in H): $\eta(\theta) = 1.037 - 0.0278\theta^2 - 0.022\theta^4$

in the range $|\theta| \leq \frac{1}{2}\pi$ (further angle segments can be obtained by continuing η symmetrically and periodically). Clearly, $\eta(\theta)$ has cusps at $\theta = \pm\frac{1}{2}\pi$ that are associated with the facets.

A totally different equilibrium morphology of the interface has been found in H(in H) configuration, where the shape of the interface was nearly circular with a small hexagonal modulation, reflecting the sixfold symmetry inside the Sm-B layers. Values of $\varepsilon \leq 0.03$ have been measured in this configuration for CCH3 (Fig.1(c).) [54], and $\varepsilon \leq 0.005$ for CCH5 [43] and these values are essentially equal with the amplitude of the basic Fourier mode $cos(6\theta)$.

In the H(in P) configuration, which has been studied for CCH5, the additional contribution to surface energy coming from the elastic deformations leads to the superposition of a twofold anisotropy of the surface tension onto the sixfold symmetry of the interface. This results in a slightly oval equilibrium shape. The analysis of the equilibrium shape by Wulff-construction gave a value for this twofold anisotropy in the range between $\varepsilon = 0.01 - 0.03$ [43].

Thermal Equilibrium in different Substances

In the P(in P) configuration for substances 3OCF3 and BCBA with different molecular structure from CCH3 a similar equilibrium shape of the interface (faceted long sides and convex short ones) has been found like that in CCH3 (Fig. 1(a)). Moreover, the shape anisotropies were similar to that in CCH3

(within the scattering described in the previous subsection). For 3OCF3 a value of $\varepsilon = 0.66$ has been measured, while in BCBA: $\varepsilon = 0.59$ [48].

In contrast, the shape anisotropy of the interface in thermal equilibrium is unexpectedly different for the three homologues of the CCHm (m=3,4,5) series. Much larger values of $\varepsilon = 0.89$ and $\varepsilon = 0.94$ have been found for CCH4 and CCH5, respectively compared to that in CCH3 ($\varepsilon = 0.68$) [42] – see Fig. 2. These considerable differences in ε for the three homologues have been interpreted by differences in the molecular packing of the Sm-B phase [42]. According to the interpretation (based on the X-ray diffraction investigations [55]), the faceted part of the interface is more rough on the molecular scale in the CCH5 compared to that in CCH4 and in CCH3 especially. Because of this roughness the packing between the N and Sm-B phases is presumably better for CCH5, which leads to a smaller surface tension on the faceted sides, and consequently to a higher anisotropy in the surface tension.

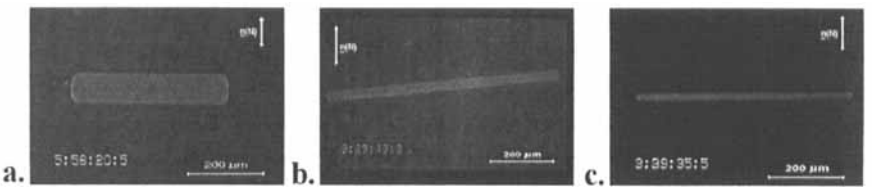

FIGURE 2 The shape of the N – Sm-B interface in thermal equilibrium (P(in P) configuration) for: (**a**) CCH3, (**b**) CCH4, (**c**) CCH5. The arrows show the director orientation in the nematic phase

The Wulff-construction gave for the angular dependence of the normalised surface tension $\eta(\theta)$ in P(in P) geometry, the following fitting functions (direction corresponding to $\theta = 0$ has been chosen parallel to the smectic layers):

in CCH3: $\eta(\theta) = 1.000 - 0.352\theta^2 + 0.008\theta^4$ [41]
in CCH4: $\eta(\theta) = 1.000 - 0.445\theta^2 + 0.026\theta^4$ [41]
in CCH5: $\eta(\theta) = 1.00 - 0.47\theta^2 + 0.03\theta^4$ [42]

in the range $|\theta| \leq \frac{1}{2}\pi$.

On the basis of the analysis of the equilibrium shape of the N – Sm-B interface, the connection of the faceted long sides to the convex short ones seems to be continuous, without any cusps in all investigated substances. It means that all surface orientations occur (no "forbidden" directions) and the surface stiffness $\sigma(\theta) + \sigma''(\theta)$ is positive everywhere (see e.g. [56]) (the only exception might be the CCH5, where the extremly large anisotropy makes difficult to analyse the Wulff plot at the critical regions). In contrast, the Sm-B – Sm-A interface was

found to be cusped at the short ends [12]. The question whether this qualitatively different behaviour of the surface tension in the two systems has some fundamental relevance is still open.

GROWTH OF THE INITIAL SMECTIC-B GERM

For small undercoolings $\Delta T < 0.2°C$ no nucleation of the Sm-B phase occured on time scales of hours. Thus, for such small undercoolings and for precise quantitative measurements we used a previously prepared Sm-B germ during several cooling-heating cycles. The procedure of obtaining the germ was similar to that described in the previous section. for thermal equilibration. In order to assure similar initial conditions, the size of the germ was fixed (always $400 - 500\mu m^2$) before applying the actual undercooling. A proper experimental procedure (described in [47]) allowed us to get a Sm-B seed with homeotropic orientation besides the planar one.

In the following subsections we describe morphological transitions depending on ΔT. In general, three growth regimes have been found as a function of ΔT, for both P(in P) and H(in H) configuration. These regimes could be distinguished by the morphology and by the growth dynamics. These growth regimes will be presented in the following subsections for the P(in P) and H(in H) configurations, while the H(in P) case is discussed in the section that deals with the heat diffusion anisotropy.

Quasi-Equilibrium Growth Regime

In a narrow range of undercoolings, typically $\Delta T \leq 0.06°C$ for planar and $\Delta T < 0.1°C$ for homeotropic Sm-B, a slow growth of the interface has been observed. Its shape has been found not much different from that in thermal equilibrium (the interface is stabilized by the surface tension in this growth regime).

In case of a planar Sm-B the long sides of the interface stay faceted, till the radius of curvature at the short (convex) sides becomes larger than in thermal equilibrium (compare Figs. 3 and 1(a)) with cusps at the locations where the convex sides connect with the facets. Such properties of the interface growth have been observed in all investigated substances, and confirmed by the computer simulations [41, 42]. The shape anisotropy of the interface increases in time (the growth velocity of the facets is smaller than that of the convex part of the interface) in both experiments and simulations. The increament of ε shows that the expansion of the already existing smectic layers is more favourable than the creation of new ones. The movement of the facets in CCH5 could be even stopped [42].

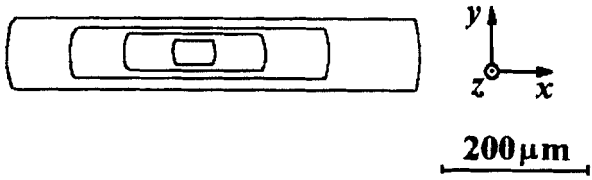

FIGURE 3 Growth morphology of the planar Sm-B germ in the quasi-equilibrium growth regime for CCH3 demonstrated by plotting the contours of the images taken at subsequent times on top of each other. $\Delta T = 0.03°C$, $t = 30s$; $90s$; $180s$; $380s$

In the quasi-equilibrium growth regime the H(in H) pattern at the beginning has a nearly circular shape with a small hexagonal modulation (see Fig. 4(a)) and in the later stage of the growth it becomes irregular – "puddle-shaped". The simulation (Fig. 4(b)) qualitatively reproduces the experiment.

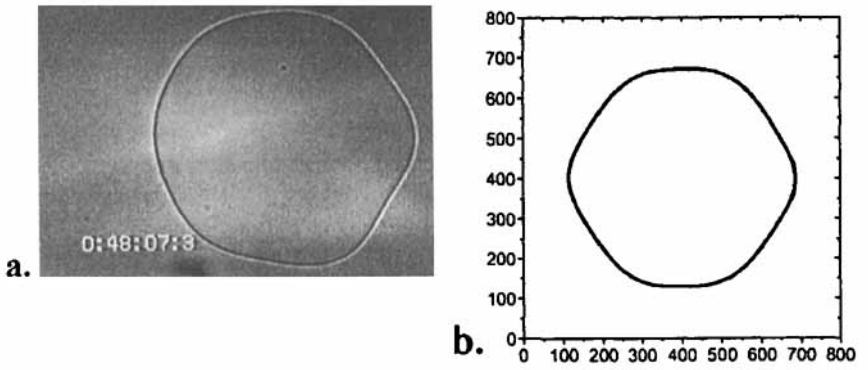

FIGURE 4 Qualitative comparison of the experimental and phase-field simulation results for CCH5 in quasi-equilibrium growth regime – H(in H) configuration. **a**. Experiment, $\Delta T = 0.05°C$. **b**. Simulation, 800×800 grid points, $\epsilon = 0.005$, $\Delta x = 0.005$, $\beta = 350$, $\Delta t = 10^{-4}$, $t = 8$, $\Delta = 0.1$, $\tau = 20$

The dynamics of the interface in this quasi-equilibrium growth regime can be understood by diffusive slowing down of a compact interface which leads to the time dependent growth velocity decreasing with t^{-C} where $C = 1/2$ – see e.g. [3]. We have measured the spatially averaged growth velocity $\frac{d\sqrt{A}}{dt}$, where A is the area of the Sm-B germ. In CCH3, at the undercoolings of $\Delta T = 0.04°C$ (P(in P) configuration), $\Delta T = 0.05°C$ (P(in H)) and $\Delta T = 0.05°C$ (H (in H)) the values of $C = 0.59$, $C = 0.52$ and $C = 0.56$ have been determined, respectively.

Intermediate Growth Regime

In the next range of undercooling i.e., for the planar Sm-B typically $0.06°C < \Delta T \leq 0.1°C$ and for the homeotropic Sm-B in the range of $0.1°C \leq \Delta T < 0.2°C$, a change in the growth morphology has been observed.

The short sides of the planar Sm-B germ became concave, but the facets still persist parallel to the Sm-B layers (Fig. 5). The destabilization of the interface is going on in this regime: four main branches are formed which grow parallel to the Sm-B layers.

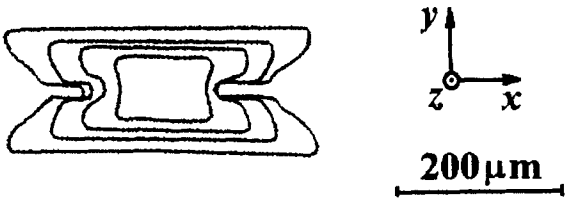

FIGURE 5 Growth morphology of the planar Sm-B germ in the intermediate growth regime for CCH3 demonstrated by plotting the contours of the images taken at subsequent times on top of each other. $\Delta T = 0.1°C$, $t = 8.4s$; $16.7s$; $26.9s$; $31.4s$

In the H(in H) geometry tips are formed and a petal shaped morphology of the interface appears (Fig. 6(a)) similarly to the experiments on the hexagonal columnar phases [57, 58]. The tips reflect the hexagonal symmetry of the Sm-B layers. For $0.1°C < \Delta T < 0.2°C$ the tips split up, but for $\Delta T = 0.2°C$ six stable dendritic tips are formed in CCH5 (see Fig. 6(c)). More or less expressed dendrites have been observed in the range of undercooling between $0.15°C$ and $0.3°C$ for CCH5.

For the dynamics of the interface in case of CCH3 we found $\frac{d\sqrt{A}}{dt} = const$ both in P(in P) and H(in H) configurations [54]. The growth rate of the perturbation has been also found constant in time for both configurations [48].

The simulations have reproduced the first destabilization of the interface for both P(in P) – [41], and H(in H) – Fig. 6(b) configurations. Moreover, for larger undercoolings the dendritic growth in the H(in H) case was also observed (Fig. 6(d)).

Fast Growth Regime

With further increase of the undercooling, for the planar Sm-B typically $\Delta T > 0.1°C$, and for the homeotropic Sm-B typically $\Delta T > 0.2°C$, a new growth regime appears.

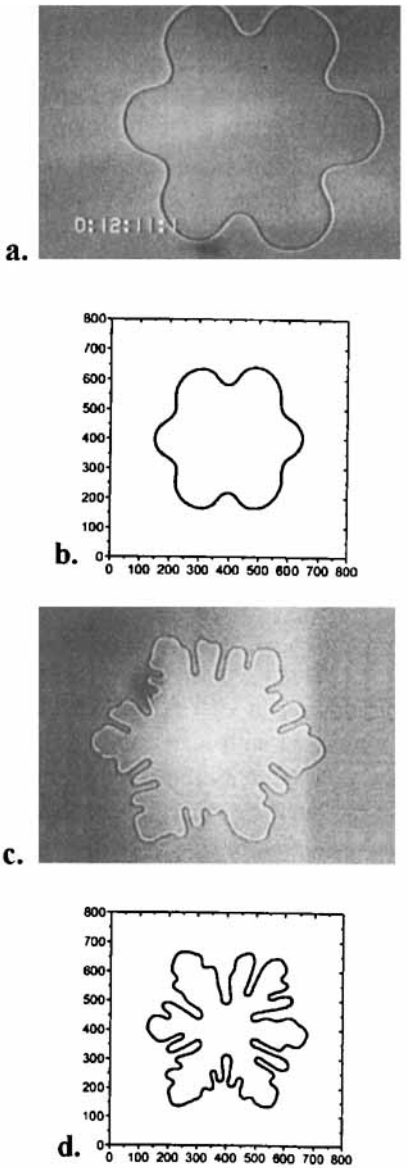

FIGURE 6 Qualitative comparison of the experimental and phase-field simulation results for CCH5 in the intermediate growth regime – H(in H) configuration. **a.** Experiment, $\Delta T = 0.1°C$. **b.** Simulation, 800 × 800 grid points. $\epsilon = 0.005$, $\Delta x = 0.005$, $\beta = 350$, $\Delta t = 10^{-4}$, $t = 2.8$, $\Delta = 0.2$, $\tau = 20$. **c.** Experiment, $\Delta T = 0.2°C$. **d.** Simulation, 800 × 800 grid points, $\epsilon = 0.005$, $\Delta x = 0.005$, $\beta = 350$, $\Delta t = 10^{-4}$, $t = 0.42$, $\Delta = 0.5$, $\tau = 20$

The morphology of the planar Sm-B changes continuously with ΔT. The facets disappear and the interface roughens up – see Fig. 7. The four main branches do not grow parallel with the Sm-B layers (as on Fig. 5), but make an angle with each other which increases in time for CCH3, and therefore the growth direction of the tips changes in time. For $\Delta T \geq 0.5°C$ one gets a dendritic growth with steady growth direction and with four main branches that enclose an angle $\approx 90°$ for CCH3. For such undercoolings the morphology of the interface is not much different from that discussed in the next section.

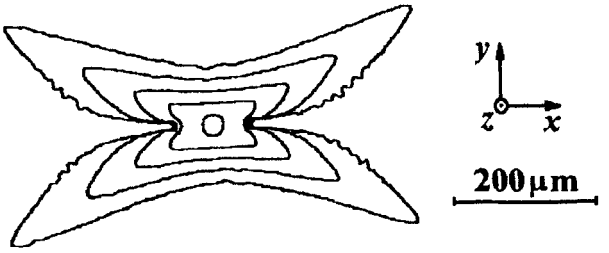

FIGURE 7 Growth morphology of the planar Sm-B germ in the fast growth regime for CCH3 demonstrated by plotting the contours of the images taken at subsequent times on top of each other. $\Delta T = 0.3°C$, $t = 0.6s$; $3.3s$; $5.7s$; $7.5s$; $10.1s$

For the H(in H) configuration in CCH5, the dendritic growth presented in Fig. 6(c) becomes less expressed with increasing the undercooling, and finally for large enough ΔT one gets the dense-branching morphology (see Fig. 8(a)). The enveloping curve of the interface preserves the hexagonal shape having the same orientation of the maxima (R_{max}) as in the quasi-equilibrium growth regime. This is in contrast to the observations made on columnar hexagonal phase [59], where the hexagonal shape of the crystal at low (surface tension controlled regime) and at high (kinetic regime) undercoolings was rotated by 30° with respect to each other. On the other hand, the experimentally observed morphological transition: compact interface – petal shape – dendritic growth – dense-branching morphology as a function of ΔT is in a good agreement with the morphological phase diagrams predicted in [60, 61].

The results of the computer simulations have clearly showed the destabilization of the facets for planar Sm-B [41] and the appearance of the dense-branching morphology with a sixfold symmetry for the homeotropic Sm-B (Fig 8(b)), as observed in the experiments.

For both, planar and homeotropic Sm-B of CCH3, $\frac{d\sqrt{A}}{dt}$ asimptotically tends to a constant value determined by ΔT [54], which is in agreement with the

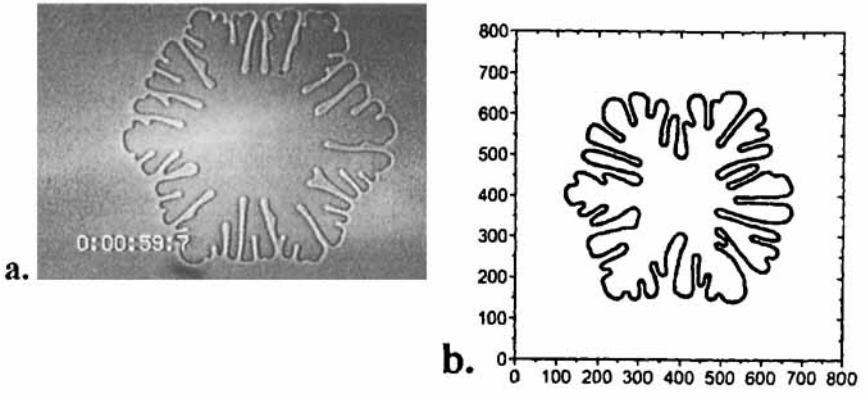

FIGURE 8 Qualitative comparison of the experimental and phase-field simulation results for CCH5 in the fast growth regime – H(in H) configuration. **a.** Experiment, $\Delta T = 0.35°C$. **b.** Simulation, 800 × 800 grid points, $\epsilon = 0.005$, $\Delta x = 0.005$, $\beta = 350$, $\Delta t = 10^{-4}$, $t = 0.25$, $\Delta = 0.6$, $\tau = 20$

generic feature of growth phenomena after the equilibrium morphology has become unstable [61, 62].

Finally, one should mention that comparison of the numerical calculations with the experimental results (Figs. 4, 6 and 8) can be made only on qualitative level due to the limitations of the phase-field model described in [38]. However, the model turned out to be quite sensitive to the anisotropies ε and $\varepsilon_{\mu 6}$. In simulations presented in Figs. 4, 6 and 8 we used $\varepsilon = 0.001$ (taken from the experimental results) and $\varepsilon_{\mu 6} = -0.003$ (which is an estimation given in [43]). Numerical calculations with these anisotropies have reproduced all the morphologies observed experimentally. However, the change of one of the anisotropies by a factor of 2 results in a pronounced modification of the growth shape, and even it can induce a morphological phase transition for some undercoolings. This sensitivity on the anisotropies is illustrated in Fig. 9 for two different undercoolings: $\Delta = 0.4$ (Fig. 9(a) and (b)) and $\Delta = 0.5$ (Fig. 9(c) and (d)). Fig. 9(b) shows the numerical results with the same parameters as in Fig. 9(a), except ε that is increased by a factor of 2. Similarly, Fig. 9(d) displays the growth shape with twice as large $\varepsilon_{\mu 6}$ as that in Fig. 9(c). Obviously, the increase of either ε or $\varepsilon_{\mu 6}$ by a factor of 2 leads to a morphological change. Patterns shown in Fig. 9(b) and (d) have expressed dendritic character that has never been observed experimentally in H(in H) configuration.

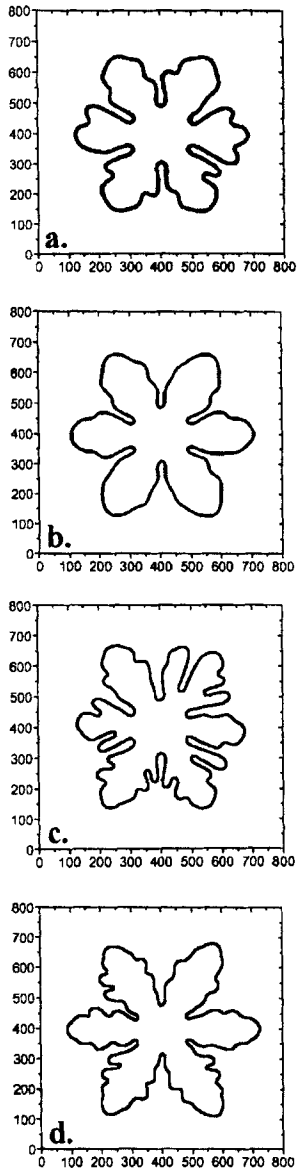

FIGURE 9 Illustration of the sensitivity of the phase-field model on the anisotropies ε and $\varepsilon_{\mu 6}$. **a.** $\Delta = 0.4$, $t = 0.8$, $\varepsilon = 0.001$, $\varepsilon_{\mu 6} = -0.003$. **b.** $\Delta = 0.4$, $t = 0.8$, $\varepsilon = 0.002$, $\varepsilon_{\mu 6} = -0.003$. **c.** $\Delta = 0.5$, $t = 0.42$, $\varepsilon = 0.001$, $\varepsilon_{\mu 6} = -0.003$. **d.** $\Delta = 0.5$, $t = 0.42$, $\varepsilon = 0.001$, $\varepsilon_{\mu 6} = -0.006$. Other phase-field parameters are as in Figs. 4, 6 and 8

HETEROGENEOUS NUCLEATION AND DENDRITIC GROWTH OF THE SMECTIC-B PHASE

The appearence of the Sm-B phase in the undercooled N takes place via heterogeneous nucleation (on some impurities, orientational defects of the director or defects on the bounding glass plates). For small undercoolings ($\Delta T < 0.2°C$) no nucleation occurred on the time scale of hours. For large enough ΔT, the fast dendritic growth of the Sm-B phase has been observed, always with planar director, independently from the orientation (planar or homeotropic) of the N environment and typically with four main dendritic branches. The growth velocity v of the dendritic tips has been found constant in time and of course undercooling dependent. The only exception is the BCBA for which $v(t) \neq const$ and which is described in [13].

Contrary to the previous section, where the morphological transition depending on ΔT has been described, in this section we compare different substances (first of all the CCHm homologues) at the same undercooling $\Delta T = 1.0°C$ in P(in P) configuration.

For quantitative characterization of the growing smectic structure the following labels were used (see also Fig. 10.): α – angle between the two closer main branches of the dendrite, which coincides with the angle between a main branch and its side-branches; γ – angle between the directors $\mathbf{n}(N)$ and $\mathbf{n}(S)$; $\mathbf{v}_1$ and $\mathbf{v}_2$ – the growth velocities of the dendritic tips.

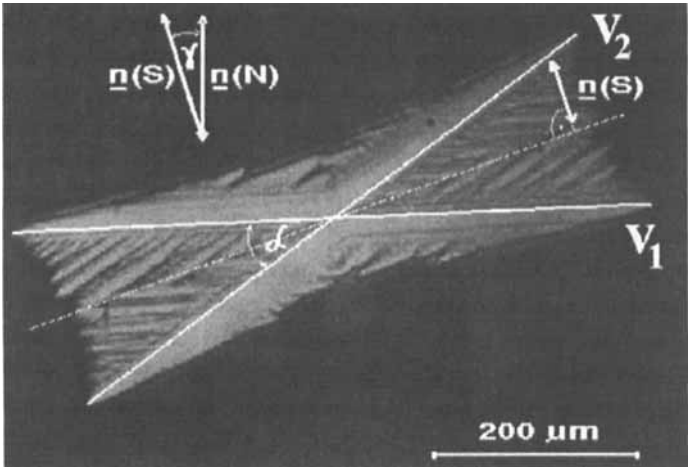

FIGURE 10 Notations used for the characterization of the Sm-B growth morphologies: $\underline{n}$(S) és $\underline{n}$(N) – director of the Sm-B and N phase, respectively; γ – the angle between the directors of the two phases; α – the (smaller) angle between the two dendritic main branches; $\mathbf{v}_1$ and $\mathbf{v}_2$ – the growth velocities of the dendritic tips

i.) In the case of CCH3 we got dendritic growth with four-fold symmetry and parabolic tips. Angle between the main branches was found $\alpha \approx 90°$ for all germs observed. Strong and symmetric side-branching activity, even of second and third generation (see Fig. 11(a)) was observed. The director of the nucleated Sm-B was parallel to the director of the surrounding nematic ($\gamma \approx 0$). In 93% of the 270 germs considered, γ was found below 5° and in the remaining 7% it was between 5° and 9°.

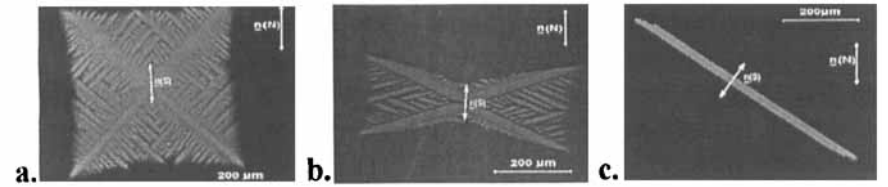

FIGURE 11 Growth morphologies of the planar Sm-B phase after heterogeneous nucleation ($\Delta T = 1.0°C$). **a.** CCH3, **b.** CCH4, **c.** CCH5. Double arrows indicate the director in both, N and Sm-B phases

ii.) For CCH4 we get dendritic-like growth, which means that the four main branches are still observable with intensive side-branching, but the tips and the length of the side-branches are not symmetric with respect to the direction of the normal growth velocity of the tip (see Fig. 11(b)). The angle between the main branches is in the range of $0° \leq \alpha \leq 60°$ and varies from germ to germ, but it does not seem to depend on the undercooling. The angle between the first generation of side branches and the main branch is always α. The angle between the nematic and smectic directors (γ) covers also a wide range: $0° \leq \gamma \leq 80°$. The distribution of γ obtained for 270 germs has been presented in [42]. A large part (~ 37%) of the germs is still oriented parallel to the $\mathbf{n}(N)$, $\gamma = 0$, but the rest is "disaligned" with respect to the nematic director, thus γ reaches values up to 80°. No germs were found with extremely large disalignment in the range of $80° < \gamma < 90°$.

No correlation between α, γ and v was found, moreover α and γ did not show any dependence on the undercooling ΔT. In general, the properties of each germ (α, γ and v) are reproducible in successive experiments provided the sample does not crystallize. But these properties can change at the same location if the sample gets into the crystalline phase and is heated up again.

iii.) For CCH5 the growing Sm-B germ has a faceted shape at any undercooling reminding its equilibrium shape, differing only at the short sides which become unstable (see Fig. 11(c)). Such a morphology can be considered as a limit $\alpha = 0°$. The directors of the N and Sm-B phases show even weaker cor-

relation than for CCH4. Though the distribution of γ is in the same angular range for different nucleation centers ($0° \leq \gamma \leq 80°$) as in CCH4, but germs with larger γ nucleate more often in CCH5 than in CCH4 i.e., the distribution of the $N(\gamma)$ (N – number of the Sm-B germs) is smoother [42]. The γ and v of the nucleated Sm-B germ at the same location in the sample might change after crystallization in the same way as it was described above for CCH4.

Computer simulations based on the phase-field model have reproduced qualitatively the growth morphologies of all three CCHm (m=3,4,5) homologues [41, 42]. The only discrepancy on the qualitative level between the experiments and simulations is that in the latter the angle α has been found noticably smaller than 90°. In order to improve the situation we should first of all incorporate the anisotropy of the kinetic term on a proper way, because computer simulations [41] showed that the angle α is very sensitive to the angular dependence of the kinetic coefficient.

The drastic change in the growth morphology of the N – Sm-B interface observed experimentally and confirmed by computer simulations in CCHm homologous series has been explained by the large difference in the surface tension anisotropy [42]. Presumably for CCH5 the surface tension anisotropy is so large (and the cusp in the angular dependence of the surface tension is so deep), that it does not allow the destabilization of the faceted sides (it would involve the appearance of the orientations that are energetically unfavoured). Only the short rough sides are destabilized as it was seen in experiments (Fig. 11(c)), contrary to the CCH4 and especially to the CCH3, where the values of ε are smaller. This idea is supported by the experiments on the 3OCF3 and BCBA which have similar ε to that of CCH3. In 3OCF3 $\alpha \approx 80°$ has been measured [48], while in BCBA $\alpha \approx 90°$ [13] with intensive side-branching activity for both substances.

The asymmetry of the side-branching activity with respect to the growth direction of the main tip in case of CCH4 (see Fig. 10.), which has been observed both experimentally and by computer simulation, could be understood by taking into account the angle between the Sm-B director and the normal to the interface. In the vicinity of the tip on that part of the interface where its normal encloses a smaller angle with the smectic director (external side – see Fig. 10.) the interface is more stable against the perturbations than on the other (internal) side. This is due to the fact that the coincidence of the surface normal and the director corresponds to the minimum in the angular dependent surface tension. Thus at this part of the interface the roughening is less expressed (any perturbation involves significant increase of the surface free energy because of large ε), compared to other parts where the angle between the surface normal and the director is larger. This is also noticeable on Figs. 10 and 11(b) where on the external side of the

dendritic tip the side branches became easely faceted, with facets parallel to the smectic layers. These phenomena are in accordance with the observation that in the process of the smectification the expansion of the already existing smectic layers is preferred instead of the creation of new ones.

PATTERN FORMATION IN BINARY MIXTURES OF CCH3 AND CCH5

In the previous section a significant difference in the growth morphologies of the Sm-B phase has been presented for the CCHm (m=3,4,5) substances. This difference has been explained by the large differences in the surface tension anisotropies for these materials. We posed a natural question whether growth morphologies detected for CCH4 (which could be interpreted as being intermediate between CCH3 and CCH5) can be "simulated" experimentally in the binary mixture of CCH3 – CCH5.

In order to answer this question mixtures of 10, 20,..., 90 mole % CCH5 in CCH3 have been prepared. In order to assure the same conditions, the similar, planarly oriented cells of thickness of $10\mu m$ have been used as for the one-component substances.

The binary mixture shows a similar phase sequence on cooling (I – N – Sm-B) in the whole concentration range as its components. The $c - T$ (concentration-temperature) diagram of the system obeys continuous mixing at high temperatures resulting in a linear $T_{NI}(c)$. On the other hand, a negative deviation (upto $10°C$) of $T_{NS}(c)$ from the additivity rule could be detected, see Fig. 12(a). The figure also indicates T_{NS} for the pure CCH4.

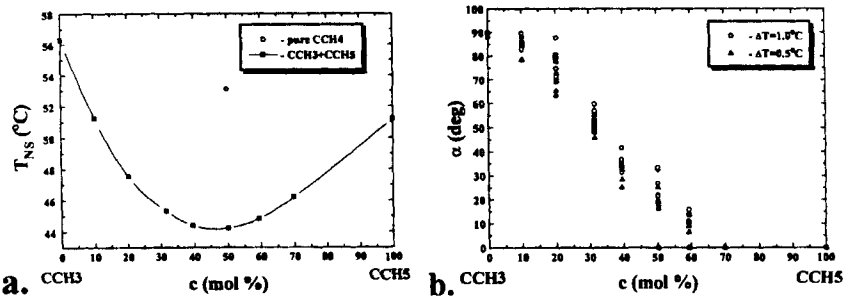

FIGURE 12 a. Temperature – concentration diagram for the binary system CCH3-CCH5. b. Concentration dependence of the angle α

The nucleation of the Sm-B phase and the pattern formation in the mixture at and below T_{NS} has been studied for different concentrations and undercoolings.

Planarly oriented growing Sm-B germs were observed in the undercooled nematic. The pattern forming behaviour of the mixture shows similarities with the one-component CCH4, which supports the idea that the mixture can be accounted for the virtual single component CCH4. In a wide concentration range (10 – 60% of CCH5) one observes dendritic-like growth, the angle between the main branches α varies from 90° to 0° in this range (see Fig 12(b)). Different values of α in Fig. 12(b) for a given concentration were obtained from different Sm-B germs and does not originate from experimental errors. Similarly to the case of the one-component CCH4, the values of α and γ depend strongly on the nucleation point. In the range of 60 – 100% of CCH5 the morphology of the growing Sm-B germ was similar to that of the pure CCH5, i.e. $\alpha = 0$ and the angle γ varied in a wide range from germ to germ.

Concerning the growth velocities v, much smaller values (by about an order of magnitude) have been found in the mixture than in the one-component materials. Due to this reduction in the tip's velocity, the side branching activity is weaker (larger wavelength, without second generation of the side branches) in the binary mixture than in one-component CCH4.

Experimental observations such as negative deviation of $T_{NS}(c)$ from the additivity rule, large temperature range of the N and Sm-B phase coexistence (up to 2°C), decrease in the tip's growth velocity by an order of magnitude compared to the one-component substances, and the increased nucleation rate show that the mixing of the two components is not ideal. Therefore, in a detailed quantitative analysis, besides the heat diffusion, we should also consider the mass transport. This leads to further complications because in liquid crystals, the mass diffusion coefficient is not only several orders of magnitude smaller than that of heat diffusion, but the mass diffusion anisotropy changes sign at the N – Sm-B transition [63], contrary to the heat diffusivity anisotropy.

THERMALLY INDUCED AGING IN CCHm COMPOUNDS

In the experiments of thermal equilibration and in the quasi-equilibrium growth regime an aging process has been observed for the CCHm homologous series, which results in a shift of phase transition temperatures and in a broadening of the phase coexistence temperature ranges.

Detailed experimental studies carried out by polarizing microscopy and DSC have shown that the air atmosphere is responsible for the thermal aging of the investigated substances. Here, we will point out only the main features of the phenomenon. The detailed discussion with the experimental results can be found in [64].

The thermal aging of the substances could be detected in the samples which were in contact with air during the experiments, or which were prepared in air atmosphere. In contrast to that, in samples which were prepared in inert gas (argon) atmosphere the aging was not observable.

The rate of the aging depends on the thermal prehistory of the sample. Optical investigations showed that the temporal drift of phase transition temperature T_{NS} is the largest (about $-0.03°C/hour$) when starting from the Cr phase and only slightly smaller (about $-0.02°C/hour$) if the cell was stored previously for one day in the Sm-B phase. Storing the cell in the N phase for one day resulted in a change (decrease) of the initial value of T_{NS} by about $0.15°C$ accompanied with a reduction of the drift (to about $-0.001°C/hour$). DSC measurements have confirmed these results showing that the temporal evolution of T_{NI} and T_{NS} follow an exponential decay and saturation. Both the total shift in T_{NI} and T_{NS} and the rate of the shift increase with the storage temperature. For e.g. cells stored in the I or N phases for a week, show a large shift of the phase transition temperatures ($5°C$ or even more) as well as a broadening of the phase coexistence ranges (up to $5°C$). The changes are more pronounced in cells stored at higher temperature (in the I phase). On the other hand, storing cells in the crystalline or Sm-B phase did not cause any remarkable change.

It should be mentioned, that the generation of impurities seems to be governed not simply by the temperature (and time) but also by the phase which the sample was stored in. Thus, a relatively small temperature difference in the storage temperature (e.g. $T_1 = T_{NS} - 1°C$ and $T_2 = T_{NS} + 1°C$), as shown in [64] causes big changes in the aging process. The determination of the actual chemical process of ageing would, however, require a more sophisticated chemical analysis.

The morphology and the dynamics of the N – Sm-B interface in aged samples differ from those seen in fresh ones too. These differences can be explained by the generation of "internal impurities" through the aging process. The concentration gradient at the SmB-N interface causes the growth to be controlled not only by the undercooling. The actual driving force of the process is a combination of the undercooling and the concentration gradient.

In the process of heterogeneous nucleation in aged cells of CCH3 at high undercoolings, the symmetry of the pattern (shown in Fig. 11(a)) is preserved, but the growing dendrite is characterised by reduced side branching activity (longer wavelength, without second generation of side branches) similarly to that discussed in the previous for the binary mixture. This is accompanied by an enormous decrease of the tip velocity (by more than an order of magnitude).

The decrease of the growth velocity in aged samples can be observed at lower undercoolings as well, but in this case it is accompanied by morphological changes too. In aged samples the faceted side of the germ becomes unstable

according to a different mechanism, instead of a uniform roughening (see Fig. 7.) a localized instability appears [48, 64]. We note here that the morphology of this latter type has already been observed previously in an other substance which is supposed to be less stable chemically [13]. Similar "grooves" on facets have been observed in directional solidification experiments too [5]. The formation of the grooves is caused there by the local increase of the impurity concentration on the liquid side of the phase boundary, which indicates again the presence of the impurities in our aged samples.

INFLUENCE OF THE HEAT DIFFUSION ANISOTROPY ON THE PATTERN FORMATION

In the experiments described in previous sections, the influence of D_a on the pattern formation could not be detected directly, and it has not been included in the discussions. Namely, for the homeotropic N the D is isotropic in the plane of the observation, while for the planar N we have discussed only the cases with $\gamma = 0$, which means that the four main branches grow symmetrically with respect to the fastest heat diffusion direction determined by $\mathbf{n}$(N). Furthermore, despite of $\gamma \neq 0$ for CCH5 in P(in P) configuration, the observed $\alpha = 0$ makes difficult the direct detection of the influence of D_a on the pattern formation.

On the other hand, for CCH4 as it was mentioned in the previous section, a large variety of growth morphologies could be experimentally observed by means of angles $0 \leq \gamma \leq 80°$ and $0 \leq \alpha \leq 60°$ (see Fig. 10. for notations). In these cases, when $\gamma \neq 0$ and $\gamma \neq 90°$, a nonreflection symmetry appeared in the growth shape (except the case of $\alpha = 0$). This means that the pair of main branches with opposite growth direction which have a larger angle with the $\mathbf{n}$(N), have larger growth velocity $|v_1|$ than the other pair ($|v_2|$) – see Fig. 10. for notations. It means that the tip's growth is preferred in the direction of the lowest heat diffusion (direction $\perp$ to $\mathbf{n}$(N)).

The observed relative difference in the growth velocities $\delta v = (|v_1| - |v_2|)/|v_1|$ in some cases reached the value of 0.2. A non-monotoneous angular dependence $\delta v(\gamma)$ has been experimentally observed with a maximum in the middle of the range $0 \leq \gamma \leq 90°$ – see Fig. 13. Taking into consideration the uniaxial nature of the nematic phase, such a behaviour is expected with $\delta v = 0$ for $\gamma = 0$ and $\gamma = 90°$ as seen in the experiments.

Note that $\eta(\theta)$ will not be modified by the elastic contribution coming from $\gamma \neq 0$ since this contribution is not θ dependent. This statement has been proved experimentally by analysing the equilibrium shape for $\gamma \neq 0$.

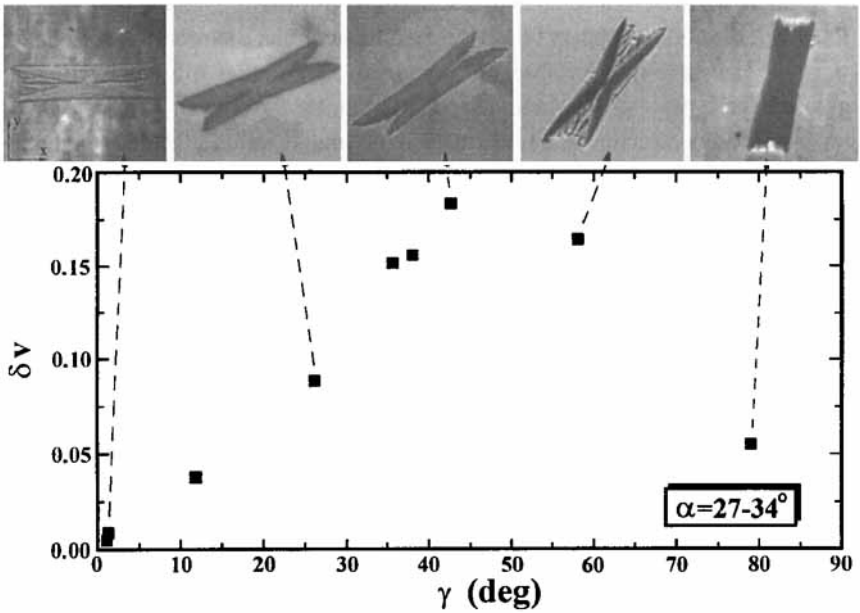

FIGURE 13 Experimental results showing the relative difference in the growth velocities $\delta v = (v_1 - v_2)/v_1$ of the main branches versus the angle γ for the Sm-B objects with angle α in a narrow range and for $\Delta T = 1.00°C$. In the upper part of the figure smectic germs with different γ are shown (the nematic director is parallel with y in each case)

On the basis of the heat diffusion anisotropy measurements [15, 16, 17] we made an estimation for D_a in CCHm (m=3,4,5) homologues [42] (preliminary measurements [65] carried out very recently on CCH5 show that the value of D_a is even larger from that estimated in [42]). The estimated value of D_a has been included into simulations based on phase-field model – see eqs. (9), (13) and (15) – in order to reproduce the growth morphologies of the interface observed in CCH4 for $\gamma \neq 0$. In these simulations with the experimentally determined $\eta(\theta)$ function (rotated by γ in the (x,y)-plane), the reflection symmetry of the growth morphology has been broken (as seen in the experiments) by including the anisotropic heat diffusion [66].

Furthermore, faster growth in the low-diffusion direction was also observed in preliminary simulation tests with only anisotropy in the thermal diffusion (neglecting the anisotropy of the surface tension) [43].

In [66] we have also shown that if the initial growth direction of the tip does not coincide with the principal axes of the heat diffusion tensor, its anisotropy influences in a certain amount the growth direction of the dendrite bending towards the lower diffusion direction.

The influence of the anisotropy in the heat diffusion has been investigated in H(in P) configuration for substance CCH5 also [43]. In this configuration, where a homeotropic Sm-B seed is surrounded by a planar N phase, an additional elastic energy is present at the interface between the two phases which involves a deformation zone in the nematic where the planar **n**(N) changes continuously to the homeotropic **n**(S). This additional contribution is similar to that mentioned in a previous section for the P(in H) configuration, and involves a twofold anisotropy of the surface tension that superposes onto the sixfold symmetry of the interface given by the hexagonal lattice inside the Sm-B layers. The surface tension function now has the form:

$$\sigma(\theta) = \sigma(0)(1 + \varepsilon_2 cos(2\theta) + \varepsilon_6 cos(6\theta)) \qquad (20)$$

where: ε_6 corresponds to the anisotropy determined for H(in H) configuration and described in a previous section. The analysis of the equilibrium shape by Wulff construction gave for the anisotropy ε_2 a value in the range between –0.01 and –0.03 [43]. It has been shown that the twofold anisotropy ε_2 causes elongation of the growing Sm-B germ in the direction parallel to **n**(N) at undercoolings investigated in [43]. Since the experimentally observed shapes of the interface show elongation in the perpendicular direction to **n**(N) (see Fig. 14(a)), obviously a different mechanism is responsible for the effect.

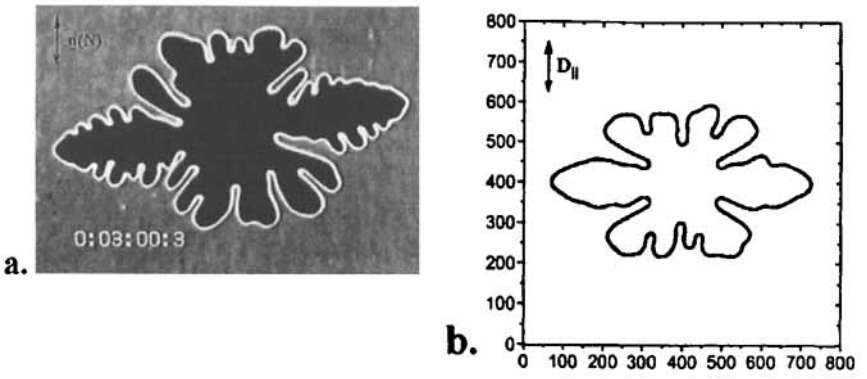

FIGURE 14 Qualitative comparison of the experimental and phase-field simulation results for CCH5 in – H(in P) configuration. **a.** Experiment, $\Delta = 0.15°C$. **b.** Simulation, 800 × 800 grid points, $\epsilon = 0.005$, $\Delta x = 0.005$, $\beta = 350$, $\Delta t = 10^{-4}$, $t = 0.36$, $\Delta = 0.5$, $\tau = 20$, $D_a = 0.2$

In H(in P) configuration the attachment kinetics of the molecules is supposed to depend on the angle enclosed by the surface normal and **n**(N). On the part of the interface, where the surface normal is perpendicular to the **n**(N), the reorientation of the director from planar to homeotropic involves twist deformation and

the kinetics should be faster than on the other parts of the interface, where the reorientation involves splay deformation mainly. This appears indeed plausible because the evolution of a twist distortion involves no backflow, in contrast to the evolution of splay [67]. Alternatively, on the molecular level, one might argue, that on the part of the interface, where the surface normal is perpendicular to the **n**(N) the molecules should only rotate in order to achieve the H orientation. On the other part of the interface, where the surface normal is parallel to the **n**(N), in addition to the rotation the mass center of the molecules should be translated, since the length of the molecules is more than 3 times larger than their diameter [55]. This effect can be described by including a twofold anisotropy $\varepsilon_{\mu 2}$ in the eq. (19), similarly to that in the surface tension (eq. (20)), and will induce an elongation of the growth shape perpendicular to **n**(N) as it has been shown in [43].

The heat diffusion anisotropy also induces an elongation of the germ and the formation of dendritic tips perpendicular to **n**(N) [43]. The experimentally observed shape presented on Fig. 14(a) has been compared with numerical simulation including the anisotropy of D only ($D_a = 0.2$, $\varepsilon_{\mu 2} = 0$) – see Fig. 14(b).

NEMATIC "ISLANDS" IN SMECTIC B MATRIX

The inverse process, namely the formation of the N phase in Sm-B on heating has been also studied. In this section the main experimental results obtained for CCH3 will be presented, while those obtained for the other substances can be found in [47, 48].

The Sm-B phase of CCH3 has a mosaic texture that consists of different planar Sm-B domains originating from different heterogeneously nucleated germs. These domains are slightly misaligned – the directors **n**(S) enclose an angle $\psi < 10°$ between different domains in the plane of observation. Such an Sm-B structure could not be overheated. Moreover, increasing the temperature nematic "islands" appear below T_{NS} (in some cases by few °C). These islands stay in equilibrium with the Sm-B for a given temperature range. With increase of the temperature in this range, the number and the size of the islands increases.

Nematic islands appear first at the domain boundary forming a channel that separates the neighbouring Sm-B domains. Experimentally has been confirmed that the "melting" temperature decreases monotonously with the increase of the angle ψ between the domains [47, 48]. This shows that the contribution of the deformation energy (which increases with ψ) to the free energy causes a decrease of the phase transition temperature. In other words, the Sm-B phase is metastable and it melts below T_{NS}.

With further increase of the temperature (but still below T_{NS}) nematic islands appear inside the Sm-B domains too, namely a small misalignment in the director's orientation can exist inside of the domain at the locations where the side branches collide with each other (see Fig. 11(a)). The most surprising feature of these islands inside a Sm-B domain is their shape. One should expect for the shape of the interface in thermal equilibrium to be the same as shown on Fig. 2(a). Contrary to the expectations, an oval (nearly elliptic) equilibrium shape has been obtained for the N islands in Sm-B matrix, with the long axis parallel to the director of the Sm-B phase (see Fig. 15(a)). The orientation of the N phase has no observable influence on the shape – its anisotropy in the range of $\varepsilon = 0.23 - 0.33$ has been found for both planar and homeotropic orientations of the N phase. The angle-dependent normalized surface tension has been determined from the equilibrium shape by Wulff plot and presented in [46].

FIGURE 15 Experimental evidence for the oval shape of the N islands in the planar Sm-B matrix in thermal equilibrium for CCH3. **a**. The shape of the N islands after thermal equilibration at $T = 55.6°C$ for $t = 5h$. **b**. The shape of the islands $t = 91.5s$ after cooling the sample to $T = 54.8°C$. **c**. The shape of the N islands after thermal equilibration at $T = 54.8°C$ for $t = 2h$

Experimental results shown on Fig. 15 gave us a direct evidence that the oval shape of the interface is really an equilibium shape. The N islands have been equilibrated for $t = 5h$ at $T = 55.6°C$. During that time the oval shape has been formed (Fig. 15(a)). After that, remaining in the temperature range of phase coexistence, the sample has been cooled to $T = 54.8°C$. Because of the growth of the Sm-B phase, the size and the shape of the N islands has been changed. After about $t = 2min$ the new volume fraction of the two phases that corresponds to the temperature $T = 54.8°C$ has been established, but the interface still remained faceted (Fig. 15(b)). However, equilibration at that temperature for $t = 2h$ caused again the formation of the oval equilibrium shape (Fig. 15(c)).

The above described experimental observation can not be completely explained by the existence of the "ordered" (without misalignment of $\mathbf{n}(S)$) and "disordered" (with small misalignment of $\mathbf{n}(S)$) Sm-B phases proposed in [46]. Namely, the appearance of the facets (Fig. 15(b)) means that the Sm-B phase is "ordered", with smaller free energy than the "disordered" one, consequently the

equilibrium shape should remain faceted, contrary to the experimental observation (Fig. 15(c)).

As a possible explanation, another effect has been considered in the analysis of the equilibrum shape of the N islands. In crystal – crystal systems (e.g. precipitates), the equilibrium shape of the second-phase particle embedded in an anisotropic, elastic matrix is strongly influenced by tensions originating from the differences in the lattice parameters of the particle and matrix (see e.g. [68]). However, in that case the equilibrium shape of the particle strongly depends on the size of the particle whereas, in our experiments the shape of the N islands remained the same by changing its linear size by about two orders of magnitude.

To explain the results presented on Fig. 15, one has to consider the *roughening transition* in the equilibrium (see e.g. [69]), which should not be mistaken for the so called kinetic roughening (see e.g. Fig. 7). This equilibrium roughening transition manifests in the dissapearance of the facets from the equilibrium shape above some critical roughening temperature T_r. Such roughening transitions have been observed in "negative crystals" (vapor bubbles included within a crystal) of diphenyl and naphtalene [70, 71]. Quite a small concentration of impurities already can lead to the roughening of the phase boundary as it has been shown in [72]. On the other hand, a small concentration of ^{3}He in ^{4}He decreases the T_r by about 20% as reported in [73].

With the above mentioned results, the experiment shown on Fig. 15 can be explained. Since our one-component substances already contain some impurities (the nominal purity of CCHm substances is > 99.5%) and taking into account the effect of thermal aging, in case of fast dendritic growth of the SmB phase, the concentration of the impurities locally increases at the locations where the side branches collide with each other. This causes a local decrease of both the T_{NS} and the T_r. Consequently, on heating of the Sm-B phase, the emerging N islands have no facets if the actual temperature is $T > T_r$ (Fig. 15(a)). By cooling the sample (containing N islands) to the temperature $T < T_r$ facets appear on the interface (Fig. 15(b)). However, in the meantime, the volume fraction of the N phase decreases i.e., the local impurity concentration increases, which again decreases T_r. After the thermodynamic equilibrium is established again, the facets disappear if the actual temperature is $T > T_r$ (Fig. 15(c)).

If one considers the equilibrium shape of a smectic germ in nematic matrix (Fig. 1(a)), the condition $T > T_r$ will not be fulfilled in the direction parallel to the Sm-B layers, since the mass transport in the N matrix is much larger than that in the Sm-B. Consequently, the impurity concentration is homogeneous in the N matrix and facets are parallel to the smectic layers (where $T < T_r$) – see e.g. Fig. 2.

The above described dependence of the "melting" temperature from the angle ψ and observations illustrated on Fig. 15, indicate that in the forming of the equilibrium shape of the "negative islands" both the structural and concentration inhomogeneities play role.

CONCLUDING REMARKS

We have presented an extended experimental investigation of the N – Sm-B interface in thermal equilibrium as well as that of the non-equilibrium growth of the free interface. The experimental results were reproduced qualitatively by computer simulations based on the phase-field model using the experimentally determined function $\eta(\theta)$ [41, 42, 66].

The fact that in thermal equilibrium the hexagonal order within the Sm-B layers does not lead to faceting of the interface in the H(in H) configuration (see Fig. 1(c)) is consistent with general principles excluding faceting in two-dimensional crystals with short-range interaction – see e.g. [74, 69]. This is presumably applicable here because the correlation of the hexagonal ordering between layers is weak. By contrast, the faceting along the Sm-B layers in P(in P) configuration (see Figs. 1(a), 1(b) and 2.) is not excluded because the extension of the facets is much larger than the molecular dimensions.

A sequence of morphological transitions: compact interface with facets (Figs. 3 and 5) – "butterfly" morphology (Fig. 7) – dendrites (Figs. 10 and 11) has been observed in the P(in P) and P(in H) configurations as a function of ΔT. In H(in H) configuration the observed morphological transition sequence was: compact interface (Fig. 4(a)) – petal shape (Fig. 6(a)) – dendrites (Fig. 6(c)) – dense-branching morphology (Fig. 8(a)).

All the basic growth morphologies have been reproduced by computer simulations based on phase-field model. Although the set of parameters used in the computer simulations might differ from the real material constants (except the $\eta(\theta)$), the qualitative resemblance is remarkably good. This resemblance (presented in [41, 42]) shows that the phase-field model is able to handle strongly anisotropic interfaces with facets in a rather simple way. Furthermore, the results show that the surface tension anisotropy is the most dominant factor in determining the morphologies in the complex growth processes observed in the experiments. We point out that computer simulations involving only the surface tension anisotropy (with isotropic heat diffusion and kinetic coefficient) have reproduced completely the qualitative picture of the experimental situation for all investigated substances. This qualitative agreement between experiments and simulations is not complete for CCH3 (which has the lowest surface tension anisotropy

among all the investigated substances) at large undercoolings only. However, details of the interface shapes at larger undercoolings depend on the kinetic term. As it was mentioned, computer simulations [41] showed that the morphology reacts sensitively to the angular dependence of the $\frac{1}{\mu(\theta)}$ at larger ΔT. A direct measurement of the kinetic coefficient would be desirable, but it would involve measuring the growth velocity at much larger undercooling than was reachable experimentally. The kinetic coefficient, including its anisotropy, has been measured for mass transport controlled growth of a hexagonal columnar mesophase [59] and the anisotropy has been estimated by numerical simulations in [43]. Another concern about the way kinetic effects are incorporated in the model relates to the fact that, when facets are present, the dependence of the kinetic term in the eq. (2) may not be strictly linear in the normal velocity. Other forms have been discussed in the literature – see e.g. [5, 75, 76]. In contrast to the anisotropy of the kinetic effects, a non-linear dependence on the velocity cannot be handled by the phase-field model in its present form, and more drastic modifications should be introduced to properly incorporate such effects. However, in view of the qualitative agreement with the experiments, these effects do not seem to affect the basic features.

We have analysed (to our knowledge for the first time) the influence of the heat diffusion anisotropy on the pattern formation. We have shown both experimentally [66] and numerically [43, 66] that the tip's growth is preferred in the lowest heat diffusion direction. Besides of the experimental and numerical methods in [43] has been shown analitically that crystal, growing in a media with anisotropic heat diffusion coefficient gets a streched shape in the low heat diffusion direction.

Acknowledgements

Investigated substances were kindly made avaliable for us by Merck, Darmstadt. The work was financially supported by research Grants No. OTKA T014957 and OTKA F022771.

References

[1] *Handbook of Crystal Growth*, edited by D. Hurle (North Holland, Amsterdam, 1993).
[2] *Solids Far from Equilibrium*, edited by C. Godrèche (Cambridge University Press, Cambridge, 1991).
[3] J. Langer, *Rev. of Modern Physics*, **52**, 1 (1980).
[4] E. Brener and V. Melnikov. *Adv. Phys.*, **40**, 53 (1991).
[5] B. Caroli, C. Caroli, and B. Roulet, in *Solids Far from Equilibrium* edited by C. Godrèche (Cambridge University Press, Cambridge, 1991), Chap. 2, p. 155.
[6] P. Noizères. in *Solids Far from Equilibrium*, edited by C. Godrèche, (Cambridge University Press, Cambridge, 1991), Chap. 1, p. 1.

[7] K. Koo, R. Ananth, and W. Gill, *Phys. Rev. A*, **44**, 3782 (1991).
[8] D. Ovsienko, G. Alfintsev, and V. Maslov, *J. Cryst. Growth*, **26**, 233 (1974).
[9] S. Huang and M. Glicksmann, *Acta Metall.*, **29**, 701 (1981).
[10] J. Bilgram, M. Firmann, and E. Huerlimann, *J. Cryst. Growth*, **96**, 175 (1989).
[11] J. Franck and J. Jung, *Physica D*, **23**, 259 (1986).
[12] P. Oswald, F. Melo, and C. Germain, *J. Phys. (Paris)*, **50**, 3527 (1989).
[13] Á. Buka and N. Éber, *Europhys. Lett.*, **21**, 477 (1993).
[14] G. Gray and J. Goodby, *Smectic Liquid Crystals* (Leonard Hill, Glasgow and London, 1984).
[15] H. Hervet, F. Rondelez, and W. Urbach, in *Liquid Crystals*, edited by S. Chandrasekhar (Heyden, London, 1980), p. 263.
[16] F. Rondelez, W. Urbach, and H. Hervet, *Phys. Rev. Lett.*, **41**, 1058 (1978).
[17] U. Zammit, M. Marinelli, R. Pizzoferrato, F. Scudieri, and S. Martellucci, *Phys. Rev. A*, **41**, 1153 (1990).
[18] W. Urbach, H. Hervet, and F. Rondelez, *J. Chem. Phys.*, **78**, 5113 (1983).
[19] P. Harrowell and D. Oxtoby, *J. Chem. Phys.*, **86**, 2932 (1987).
[20] D. Oxtoby, in *Liquids, Freezing, and the Glass Transition*, edited by J.-P. Hansen, D. Levesque, and J. Zinn-Justin (North-Holland, Amsterdam, 1991).
[21] B. Halperin, P. Hohenberg, and S.-K. Ma, *Phys. Rev. B*, **10**, 139 (1974).
[22] P. Hohenberg and B. Halperin, *Rev. Mod. Phys.*, **49**, 435 (1977).
[23] J. Langer, in *Directions in Condensed Matter Physics*, edited by G. Grinstein and G. Mazenko (World Scientific, Singapore, 1986) p. 164.
[24] G. Caginalp, *Phys. Rev. A*, **38**, 5887 (1989).
[25] G. McFadden, A. Wheeler, R. Braun, S. Coriell, and R. Sekerka, *Phys. Rev. E*, **48**, 2016 (1993).
[26] M. Gurtin, in *Metastability and Incompletely Posed Problems*, edited by S. Antman, J. Ericksen, D. Kinderlehrer, and I. Müller (Springer-Verlag, Berlin, 1987).
[27] P. Fife and G. Gill, *Physica D*, **35**, 267 (1989).
[28] P. Fife and G. Gill, *Phys. Rev. A*, **43**, 843 (1991).
[29] H. Löwen, J. Bechhoefer, and L. Tuckerman, *Phys. Rev. A*, **45**, 2399 (1992).
[30] G. Fix, in *Free-Boundary Problems: Theory and Applications*, edited by A. Fasano and M. Primicerio (Pitman, Boston, 1983).
[31] J.-T. Lin, in *PhD thesis* (Dept. of Math., Carnegie Mellon University, 1984).
[32] S. Schofield and D. Oxtoby, *J. Chem. Phys.*, **94**, 2176 (1991).
[33] G. Caginalp and E. Socolovsky, *J. Comp. Phys.*, **95**, 85 (1991).
[34] R. Kobayashi, *Bull. Jpn. Soc. Ind. Appl. Math.*, **1**, 22 (1991).
[35] R. Kobayashi, *Physica D*, **63**, 410 (1993).
[36] R. Kobayashi, in *Pattern Formation in Complex Dissipative Systems*, edited by S. Kai (World Scientific, Singapore, 1992).
[37] A. Wheeler, B. Murray, and R. Schaefer, *Physica D*, **66**, 243 (1993).
[38] A. Karma and W.-J. Rappel, *Phys. Rev. E*, **53**, R3017 (1996).
[39] A. Karma and W.-J. Rappel, *Phys. Rev. Lett.*, **77**, 4050 (1996).
[40] S.-L. Wang, R. Sekerka, A. Wheeler, B. Murray, R. Braun, S. Coriell, and G. McFadden, *Physica D*, **69**, 189 (1993).
[41] R. González-Cinca, L. Ramirez-Piscina, J. Casademunt, A. Hernández-Machado, T. Tóth-Katona, T. Börzsönyi, and Á. Buka, *Physica D*, **99**, 359 (1996).
[42] T. Tóth-Katona, T. Börzsönyi, Z. Váradi, J. Szabon, Á. Buka, R. González-Cinca, L. Ramirez-Piscina, J. Casademunt, and A. Hernández-Machado, *Phys. Rev. E*, **54**, 1574 (1996).
[43] T. Börzsönyi, A. Buka, and L. Kramer, *Phys. Rev. E*, **58**, 3236 (1998).
[44] L. Sallen, P. Oswald, J. Gèminard, and J. Malthete, *J. Phys. II. France*, **5**, 937 (1995).
[45] G. Wulff, *Z. Kristallogr. Mineral.*, **34**, 449 (1901).
[46] Á. Buka, T. Tóth Katona, and L. Kramer, *Phys. Rev. E*, **49**, 5271 (1994).
[47] T. Tóth Katona and Á. Buka, *Mol. Cryst. Liq. Cryst*, **261**, 349 (1995).
[48] T. Tóth-Katona, in *PhD thesis* (University Eötvös Loránd, Budapest, 1998).
[49] M. Muschol, D. Liu, and H. Cummins, *Phys. Rev. A*, **46**, 1038 (1992).
[50] M. Glicksmann and N. Singh, *J. Cryst. Growth*, **98**, 277 (1989).
[51] A. Dougherty, *J. of Crystal Growth*, **110**, 501 (1991).
[52] E. Rubinstein and M. Glicksman, *J. of Crystal Growth*, **112**, 97 (1991).
[53] J. Géminard and P. Oswald, *Phys. Rev. E*, **55**, 4442 (1997).

[54] Á. Buka, T. Tóth Katona, and L. Kramer, *Phys. Rev. E*, **51**, 571 (1995).
[55] R. Brownsey and A. Leadbetter, *J. Phys. Lett.*, **42**, 135 (1981).
[56] R. Kern, in *Morphology of crystals*, edited by I. Sunagawa (Terra Scientific Publishing Company, Tokyo, 1987), Chap. 2, p. 79.
[57] P. Oswald, *J. Phys. (Paris)*, **49**, 2119 (1988).
[58] P. Oswald, J. Malthéte, and P. Pelcé, *J. Phys.*, **50**, 2121 (1989).
[59] J. Géminard, P. Oswald, D. Temkin, and J. Malthête, *Europhys. Lett.*, **22**, 69 (1993).
[60] E. Ben-Jacob and P. Garik, *Physica D*, **38**, 16 (1989).
[61] E. Ben-Jacob and P. Garik, *Nature*, **343**, 523 (1990).
[62] E. Brener, H. Müller-Krumbhaar, and D. Temkin, *Europhys. Lett.*, **17**, 535 (1992).
[63] G. J. Krüger, *Phys. Rep.*, **82**, 231 (1982).
[64] T. Tóth-Katona, N. Éber, and Á. Buka, *Mol. Cryst. Liq. Cryst.*, **328**, 467 (1999).
[65] M. Marinelli, private communication.
[66] R. González-Cinca, L. Ramirez-Piscina, J. Casademunt, A. Hernández-Machado, T. Tóth-Katona, T. Börzsönyi, and Á. Buka, *J. of Cryst. Growth*, **193**, 712 (1998).
[67] S. Chandrasekhar, *Liquid Crystals* (Cambridge University Press, Cambridge, 1992).
[68] M. Thompson, C. Su, and P. Voorhees, *Acta Metall. Mater.*, **42**, 2107 (1994).
[69] H. van Beijeren and I. Nolden, in *Structure and Dynamics of Surfaces II*, edited by W. Schommers and P. van Blankenhagen (Springer-Verlag, Berlin, 1987), p. 259.
[70] A. Pavlovska and D. Nenow, *Surf. Sci.*, **27**, 211 (1971).
[71] A. Pavlovska and D. Nenow, *J. Cryst. Growth*, **12**, 9 (1972).
[72] D. Huse and C. Henley, *Phys. Rev. Lett.*, **54**, 2708 (1985).
[73] Y. Carmi, E. Polturak, and S. Lipson, *Phys. Rev. Lett.*, **62**, 1364 (1989).
[74] M. Wortis, in *Proceedings of the 1984 Trondheim Summer School*, edited by E. Cohen (North Holland, Amsterdam, 1985) p. 87.
[75] P. Oswald and F. Melo, *J. Phys. II (France)*, **2**, 1345 (1992).
[76] E. Raz, S. Lipson, and E. Polturak, *Phys. Rev A*, **40**, 1088 (1989).